SITE EVALUATION USING LUNAR SHABAR

Pan-STARRS Internal Memo

January 23, 2004

Abstract

We consider the possibility of characterizing the low altitude contribution to the seeing at potential Pan-STARRS sites using lunar shadow band ranging (SHABAR). We show how the shadow band spatial correlation function (SBSCF) can be computed in the geometric optics limit of wave optics (and clarify the assumptions under which this is valid). For a circular disk we recover Beckers' results, though with a slightly different window function. The formulation developed here applies for an extended object of arbitrary shape, allowing one treat the moon (which is highly non-uniform). We show the relation between the SBSCF and the seeing and we also model the form of the spatio-temporal correlation function. We discuss confusion with other sources of correlated intensity fluctuations. We show how the scintillation strength profile, and hence $C_n^2(h)$, can be recovered from the SBSCF obtained from a linear SHABAR array by a regularized inversion algorithm that can be implemented as a direct convolution of the SBSCF, and we discuss the relation between this and the Weiner filter for this problem. We also present an approximate inversion algorithm that is a smoothed second derivative of the 1-D SBSCF. We discuss signal to noise issues.

Revision History:
2003/11/08 NK. First cut at intro and analysis.
2003/11/14 NK. Added real lunar images + simple $C_n^2(h)$ estimator.
2003/11/29 NK. Added Fourier inversion + elaborated on simple inversion algorithm

Contents

1 Introduction

'Shadow Band Ranging' (SHABAR) uses the correlation between scintillometers bathed in light from extended objects to probe the profile of seeing inducing atmospheric refractive index fluctuations at low altitude (Seykora (1993); Beckers (1993)). SHABAR exploits the fact that the size, and therefore also the brightness, of an extended object seen through a layer of turbulence will fluctuate with time. If the layer is at distance z, and the angular diameter of the object is Ω then the fluctuations measured by two scintillometers a distance d apart will be strongly correlated if $d < \Omega z$ and *vice versa*. From measurements of correlations at separations of 1cm to 1m using the moon should allow one to probe the profile of the boundary layer on scales from of order 1m to several hundred m.

Solar SHABAR has been used effectively for site testing for the ATST (Beckers, 2001). Hickson (private communication) has successfully performed lunar SHABAR measurements. SHABAR analysis could potentially be very useful for Pan-STARRS in comparing Mauna-Kea and Haleakala since these sites presumably have almost identical high-altitude seeing. It may also be useful during operations as a probe of local sources of seeing.

2 Analysis

Beckers (1993) uses the Roddier (1981) formula for the scintillation of a point source as observed through a telescope with a simple circular aperture of diameter D in the geometric optics limit: $D \gg \sqrt{\lambda z}$ where z is the distance of the refractive fluctuations. Beckers assumes that the scintillation for an extended disc of angular diameter Ω as measured by a scintillometer of diameter $D_{\rm det}$ is given by the same formula, but with D replaced by $D + z\Omega$. As we shall see, that is not quite correct.

Hickson and Lanzetta (Hickson, personal communication) start from wave optics, but assume at the outset that the phase error introduced by the atmosphere is small. This assumption was also used by Hill, Radick and Collados (http://atst.nso.edu/site/reports.html) in their C_n^2 analysis for the ATST site survey. This assumption is commonly used to analyze scintillation of point sources, where the relevant scale — the Fresnel scale $r_f = \sqrt{h\lambda} \sim 5{\rm cm}(h/5{\rm km})^{1/2}(\lambda/0.5\mu{\rm m})^{1/2}$ — is small compared to the Fried scale r_0 (in good conditions at least). However for extended objects, and except for very altitude fluctuations, this is too restrictive. At distance z, an object of angular diameter Ω projects to a disk of diameter $D = h\Omega$ whereas the phase difference across that scale is $\delta\varphi = \sqrt{S_\varphi(D)} = \sqrt{6.88}(\Omega z/r_0)^{5/6}$ which is small compared to unity only for distances $z \lesssim 7{\rm m}(r_0/20{\rm cm})(0.01/\Omega)$.

Here, following Hickson and Lanzetta, we start from diffraction theory, and show how the shadow band correlation function for an extended object can be related to the power spectrum of the atmospheric wavefront corrugations in the geometric optics limit, and further assuming that the fractional intensity fluctuations are small, but without the restriction on the phase errors be small.

2.1 Linear Geometric Optics Limit of Wave Optics

Consider first the intensity of radiation from a distant point source arriving at a plane at $z = 0$ oriented perpendicular to the source direction. Refractive index fluctuations along the light path at distance z will introduce a phase error $\varphi(\mathbf{x})$, so the electric field of the emerging wave will be $E(\mathbf{x}, z) \propto e^{i\varphi(\mathbf{x})}$. Here $\mathbf{x}$ denotes physical separation perpendicular to the light path. According to diffraction theory, the complex field at position $\mathbf{x}$ on the $z = 0$ plane is, modulo an uninteresting constant phase factor,

$$E(\mathbf{x}, 0) = \frac{1}{i\lambda z} \int d^2x'\ E(\mathbf{x}', z) e^{i\pi|\mathbf{x}-\mathbf{x}'|^2/\lambda z} \tag{1}$$

or $E(\mathbf{x}, 0) = E(\mathbf{x}, z) \star G(\mathbf{x})$ with $G(\mathbf{x}) = \exp(i\pi x^2/\lambda z)/i\lambda z$. Now the Fourier transform of G is $\tilde{G}(\mathbf{k}) = \int d^2x\ G(\mathbf{x}) \exp(i\mathbf{k}\cdot\mathbf{x}) = \exp(-ik^2 z\lambda/4\pi)$, so, from the convolution theorem, the spatial transform of the field is

$$\tilde{E}(\mathbf{k}, 0) = \tilde{E}(\mathbf{k}, z) e^{-ik^2 z\lambda/4\pi}. \tag{2}$$

We recognize, in the argument of the exponential, the square of the product of the spatial frequency of the refractive index fluctuations k and the Fresnel scale $r_F = \sqrt{z\lambda}$.

For refractive index fluctuations at spatial frequency k such that

$$k^2 z\lambda \ll 1 \tag{3}$$

we can expand the exponential in (2) to give

$$\tilde{E}(\mathbf{k}, 0) = \tilde{E}(\mathbf{k}, z)(1 - ik^2 z\lambda/4\pi + \ldots) \tag{4}$$

where $\ldots$ denotes terms of order $(k^2 z\lambda)^2$ or higher. Equivalently, in real space,

$$E(\mathbf{x}, 0) = E(\mathbf{x}, z)\left(1 + \frac{iz\lambda}{4\pi}\frac{\nabla^2 E(\mathbf{x}, z)}{E(\mathbf{x}, z)} + \ldots\right). \tag{5}$$

Here ∇^2 denotes the two dimensional Laplacian operator. With $E(\mathbf{x}, x) = \exp(i\varphi(x))$, this becomes

$$E(\mathbf{x}, 0) = E(\mathbf{x}, z)\left(1 + \frac{z\lambda}{4\pi}(\nabla^2\varphi + i|\nabla\varphi|^2) + \ldots\right), \tag{6}$$

and the normalized irradiance is

$$I(\mathbf{x}) = \frac{|E(\mathbf{x}, 0)|^2}{|E(z)|^2} = 1 + \frac{z\lambda}{2\pi}\nabla^2\varphi + \ldots \tag{7}$$

where we have further assumed that

$$k^2 z\lambda\varphi_k \ll 1. \tag{8}$$

Here φ_k is the typical phase fluctuation generated by fluctuations on scale k. Since the phase error $\varphi_k = 2\pi\eta/\lambda$, where $\eta(\mathbf{x})$ is the wavefront deviation, we can also write the intensity as $I = 1 + \delta I$ with

$$\delta I(\mathbf{x}) = z\nabla^2\eta + \ldots \tag{9}$$

which we recognize as the linearized (i.e. small amplification, no caustics) limit of geometric optics.

Thus provided both conditions (3; geometric optics) and (8; linearity) hold there is a very simple linear relationship between the measurable intensity and the wavefront corrugations imposed by the atmosphere. We shall presently show that both of these conditions hold to a very good approximation for those spatial frequencies that are responsible for lunar scintillation.

2.2 Finite Source and Detector Size

Equation (9) applies for a point source and a point like detector. If the detector has finite size, the intensity fluctuations measured are the true fluctuations convolved with an appropriate window function. Furthermore, if the source has a finite size, this is equivalent to what would be seen for a sum of incoherent point sources, so this introduces a smoothing with a window function $W_{\rm src}(\mathbf{x})$:

$$\overline{\delta I}(\mathbf{x}) = h\sec(\zeta) W_{\rm det}(\mathbf{x}) \star W_{\rm src}(\mathbf{x}) \star \nabla^2\eta(\mathbf{x}) \tag{10}$$

where we have replaced z by $h\sec\zeta$ with ζ the zenith angle and h the altitude. For observations of the full moon, for example, $W_{\rm src}(\mathbf{x})$ is a disc of diameter $D_{\rm src} = h\Omega\sec\zeta$. However, even in this case the double convolution is not quite the same as convolving with a single disk of radius $D_{\rm src} + z\Omega$ as assumed by Beckers. The source window function for an arbitrary source can be obtained from an image.

The intensity fluctuation is then simply the convolution of the Laplacian of the wavefront deformation $\eta(\eta)$ with the detector and source window functions. Now for Kolmogorov turbulence, $\eta(\mathbf{x})$ has power spectrum $\propto k^{-11/3}$ so the Laplacian has power spectrum $\propto k^{1/3}$. This is quite close to white noise, so one might expect that the correlation function to be simply proportional to the overlap integral, and this is indeed quite a good approximation. As we will see, the main effect of the slight non-flatness of the spectrum results in a slight anti-correlation at lags just beyond overlap.

2.3 Equal Time SHABAR Correlation Functions

For a single refractive layer, the equal-time correlation funtion for two scintillometers with separation perpendicular to the source direction $\mathbf{d}$ is

$$\xi(\mathbf{x}) \equiv \langle \overline{\delta I}_1 \overline{\delta I}_2 \rangle_{\mathbf{x}} = h^2 \sec^2\zeta \int \frac{d^2k}{(2\pi)^2} P_\eta(k) k^4 |\widetilde{W}_{\rm src}(\mathbf{k})|^2 |\widetilde{W}_{\rm det}(\mathbf{k})|^2 e^{i\mathbf{k}\cdot\mathbf{x}}. \tag{11}$$

where, $\langle \tilde\eta(\mathbf{k})\tilde\eta^\star(\mathbf{k}')\rangle = (2\pi)^2\delta(\mathbf{k}-\mathbf{k}')P_\eta(k)$ and, according to Kolmogorov theory, the 2-D power spectrum for the wavefront deformation arising from a slab of turbulence is $P_\eta(k) = \alpha\Delta h \sec\zeta C_n^2(h) k^{-11/3}$ where α is a constant. Summing over multiple layers yields

$$\xi(\mathbf{x}) = \alpha \sec^3\zeta \int dh\; C_n^2(h) h^2 \int \frac{d^2k}{(2\pi)^2} k^{1/3} |\widetilde{W}_{\rm src}(\mathbf{k})|^2 |\widetilde{W}_{\rm det}(\mathbf{k})|^2 e^{i\mathbf{k}\cdot\mathbf{x}}. \tag{12}$$

We can now ask whether the conditions assumed above actually apply. Approximating the source as a uniform disk with a sharp edge, the window functions here are constant for $k \lesssim 1/D$ and fall off as $1/k^3$ for $k \gtrsim 1/D$. If the refractive layer lies at altitude $z \gg D_{\rm det}/\Omega$ then the source window cuts in before the detector window function (which can therefore be ignored), and, for zero lag ($d = 0$), the integral over spatial frequency is dominated by frequencies around $k \sim 1/(z\Omega)$, so $k^2 z\lambda \simeq \lambda/z\Omega^2$. This falls off with increasing height, and, at $z \sim D_{\rm det}/\Omega$, the lower limit of its domain of applicability, $k^2 z\lambda \sim \lambda/(D_{\rm det}\Omega) = 5\times 10^{-3}\lambda_{0.5}/D_{\rm det,0.01}\Omega_{0.01}$ where $\lambda_{0.5}$ is the wavelength in units of 0.5μm, $D_{\rm det,0.01}$ is the detector diameter in cm, and $\Omega_{0.01}$ is the angular diameter in units of 0.01 radians. Evidently, $k^2 z\lambda$ is very small, so geometric optics should provide a good approximation. The phase fluctuations on scale k are on the order $\varphi \sim \sqrt{6.88}(kr_0)^{-5/6}$, so $k^2\lambda z\varphi \sim (\lambda/r_0)\Omega^{-7/6}(r_0/z)^{1/6}$. This is again a decreasing function of altitude, and at $z \sim D_{\rm det}/\Omega$ we have $k^2\lambda z\varphi \sim 2.5(\lambda/r_0)\Omega^{-1}(r_0/D_{\rm det})^{1/6} \sim 10^{-3}\lambda_{0.5} r_{0,0.3}^{-5/6} D_{\rm det,0.01}^{-1/6}\Omega_{0.01}^{-1}$, where $r_{0,0.3}$ is the Fried length in units of 0.3m. This again is very small, so the assumption of linearity is very good indeed.

For a detector size on the order of one cm, and for refractive fluctuations at heights greater than a meter, we can ignore the smoothing with the detector window, and we have $\widetilde{W}_{\rm src}(\mathbf{k}) = \widetilde{W}_p(\mathbf{k}\Omega h\sec\zeta)$ where $\widetilde{W}_p(\mathbf{k})$ is the transform of the normalized shape of the moon at phase p, scaled to have unit diameter. We can then write the auto-correlation function as

$$\xi(\mathbf{x}) = \frac{\alpha\Omega^{-7/3}\sec^{2/3}\zeta}{(2\pi)^2} \int dh\; C_n^2(h) h^{-1/3} \xi_0(x/\Omega h\sec\zeta) \tag{13}$$

where

$$\xi_0(\mathbf{x}) = \int d^2y\; y^{1/3} |\widetilde{W}_p(\mathbf{y})|^2 e^{i\mathbf{y}\cdot\mathbf{x}} \tag{14}$$

which, for the case of a featureless circular disk, is equivalent to Beckers' result.

2.4 Relation to the Seeing

The structure function for phase fluctuations is

$$S_\varphi(x) = \langle(\varphi(\mathbf{x}) - \varphi(0))^2\rangle = (2\pi/\lambda)^2\alpha\sec\zeta \int dh\; C_n^2(h) \int \frac{d^2k}{(2\pi)^2} k^{-11/3} 4\sin^2(\mathbf{k}\cdot\mathbf{x}/2). \tag{15}$$

This is conventionally written as $S_\varphi(x) = 6.88(x/r_0)^{5/3}$, and the Fried length is related to the width of the seeing disk by FWHM $\simeq 0.98\lambda/r_0$, so the image quality is related to $C_n^2(h)$ by

$$\mathrm{FWHM}^{5/3} = \frac{4}{6.88}\lambda^{-1/3}\alpha\sec\zeta \int dh\; C_n^2(h) \int d^2y\; y^{-11/3}\sin^2(\hat{\mathbf{x}}\cdot\mathbf{y}/2). \tag{16}$$

It is interesting to compare (13) and (16). Some notable features are:

- The $C_n^2(h)$ integral has a slightly different weighting; for a given amount of seeing, the SHABAR fluctuations amplitude scales as $h^{-1/6}$, so high altitude seeing will produce smaller scintillation. A more powerful discriminator, however, is the dependence on spatial separation. Another useful discriminator is the time-scale for the fluctuations, which is shorter for lower altitude refraction.

- The SHABAR signal increases more slowly with zenith angle than the seeing.

- The SHABAR relative intensity fluctuations will be larger for observations of the crescent moon, with the covariance scaling inversely as the width of the crescent. For photon counting limited observations, the signal to noise is independent of the phase.

- The SHABAR signal is independent of the wavelength, while the seeing width has the familiar $\lambda^{-1/5}$ dependence.

It is also interesting to ask: How sensitive is the predicted ratio of seeing to SHABAR fluctuation strength to the assumption of Kolmogorov scaling? For high altitude seeing, this can be an important issue. The width of the seeing disk depends primarily on fluctuations on the Fried scale r_0, with is on the order of tens of cm, while the SHABAR fluctuations probe the refractive index on the order of ten (one hundred) m for fluctuations at 1 (10) km altitude. These scales are very different, and the latter may be beyond the outer scale. However, for fluctuations at an altitude of a few tens of m, the SHABAR fluctuations are directly probing the same scales as are responsible for the seeing, so the comparison should be relatively insensitive to departures from pure Kolmogorov scaling.

Taking the ratio of (13) at zero lag ($\mathbf{d} = 0$) and (16) for a single refractive layer yields

$$\frac{\xi(0)}{(\mathrm{FWHM})^{5/3}} = \frac{6.88}{16\pi^2}\Omega^{-7/3}\sec^{-1/3}\zeta\left(\frac{\lambda}{z}\right)^{1/3}\frac{\int d^2y\; y^{1/3}|\widetilde{W}_p(\mathbf{y})|^2}{\int d^2y\; y^{-11/3}\sin^2(\hat{\mathbf{x}}\cdot\mathbf{y}/2)} \tag{17}$$

For full moon, we find $I_1 = \int d^2y\; y^{1/3}|\widetilde{W}_p(\mathbf{y})|^2 \simeq 81$ while $I_2 = \int d^2y\; y^{-11/3}\sin^2(\hat{\mathbf{x}}\cdot\mathbf{y}/2) \simeq 2.5$, from which we obtain

$$\xi(0) = 3.5\times10^{-7}(z/10\mathrm{m})^{-1/3}(\mathrm{FWHM}/1''.0)^{5/3} \tag{18}$$

in good agreement with Beckers' results.

For the crescent moon the window function has a greater bandwidth and, for a crescent of width one fifth of the lunar diameter, $I_1 \simeq 630$ and the zero-lag auto-correlation function for the fiducial 1 arcsec seeing layer at 10 m altitude, 2.5×10^{-6}. The shadow band auto-correlation function is shown for a selection of phase angles in figure 1. Note how the width of the auto-correlation function decreases for the crescent moon, especially in the direction toward the sun. A surface plot the the SBSCF for the full moon is shown in figure 2.

2.5 Spatio-Temporal Correlation Function

In the 'frozen-flow' approximation, $\eta(\mathbf{x},t) = \eta(\mathbf{x}-\mathbf{v}t)$, and the spatio-temporal autocorrelation function is $\xi(\mathbf{x},t) = \xi_0(\mathbf{x}-\mathbf{v}t)$. Here $\mathbf{v} = (v_x, v_y)$ is related to the true velocity $\mathbf{v}'$ by $\mathbf{v} = (v_x', v_y'\cos\zeta)$ where subscripts x and y denote the azimuthal and altitude components. This model predicts that measurements of the spatial correlation function at a finite time-lag should be offset by a distance $\mathbf{v}\Delta t$. If the wind velocity is known, this provides a check on the reality of the signal (though this would not discriminate against false signals arising from patchy dust or mist extinction). This also tells us what time sampling is needed (or how much the signal will be reduced if we have too long an averaging time). For a wind speed on the order of 10 m/s, the time-scale is $\tau \sim h\Omega/v \simeq 10\mathrm{ms}h_1 0$.

The frozen-flow approximation will only hold for time-lags less than the turnover time $\tau_\star$ for eddies of the approriate size. According to Kolmogorov theory, the turnover time scales as the 2/3 power of the eddy size, and it follows that $\tau_\star \sim (r_{\mathrm{outer}}/\Omega h)^{1/3}\tau$. For boundary layer fluctuations it is reasonable to assume that the outer scale is approximately the same as the height, so $\tau_\star/\tau \sim \Omega^{-1/3}$, or equivalently that the persistence time for an eddy is around 5 times the fluctuation time-scale.

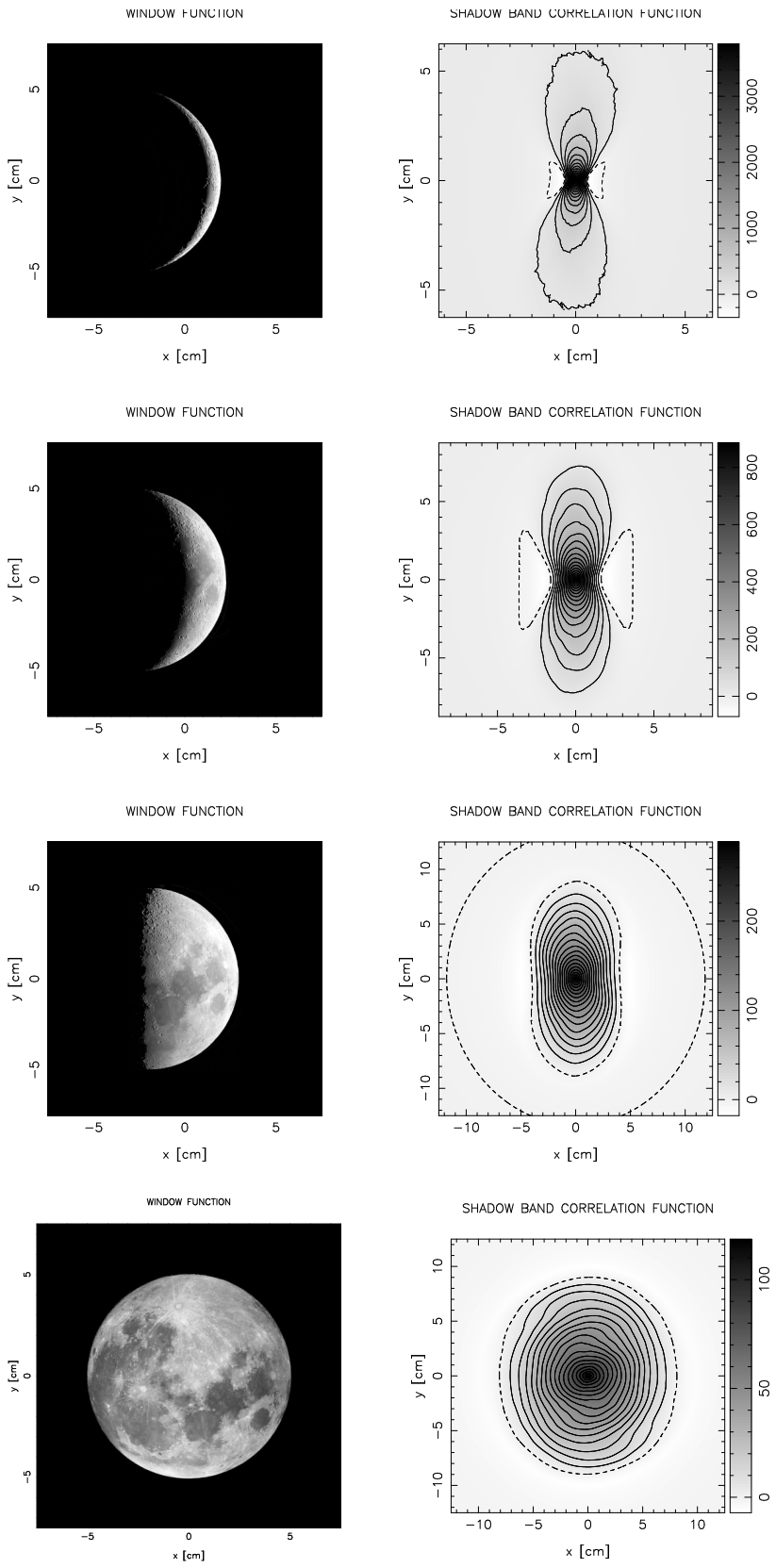

Figure 1: Window functions and shadow-band autocorrelation function. Length scales assume an altitude of 10m and scale linearly with altitude. Note the different z-scale and also the different length scale for the crescent moon correlation funnction.

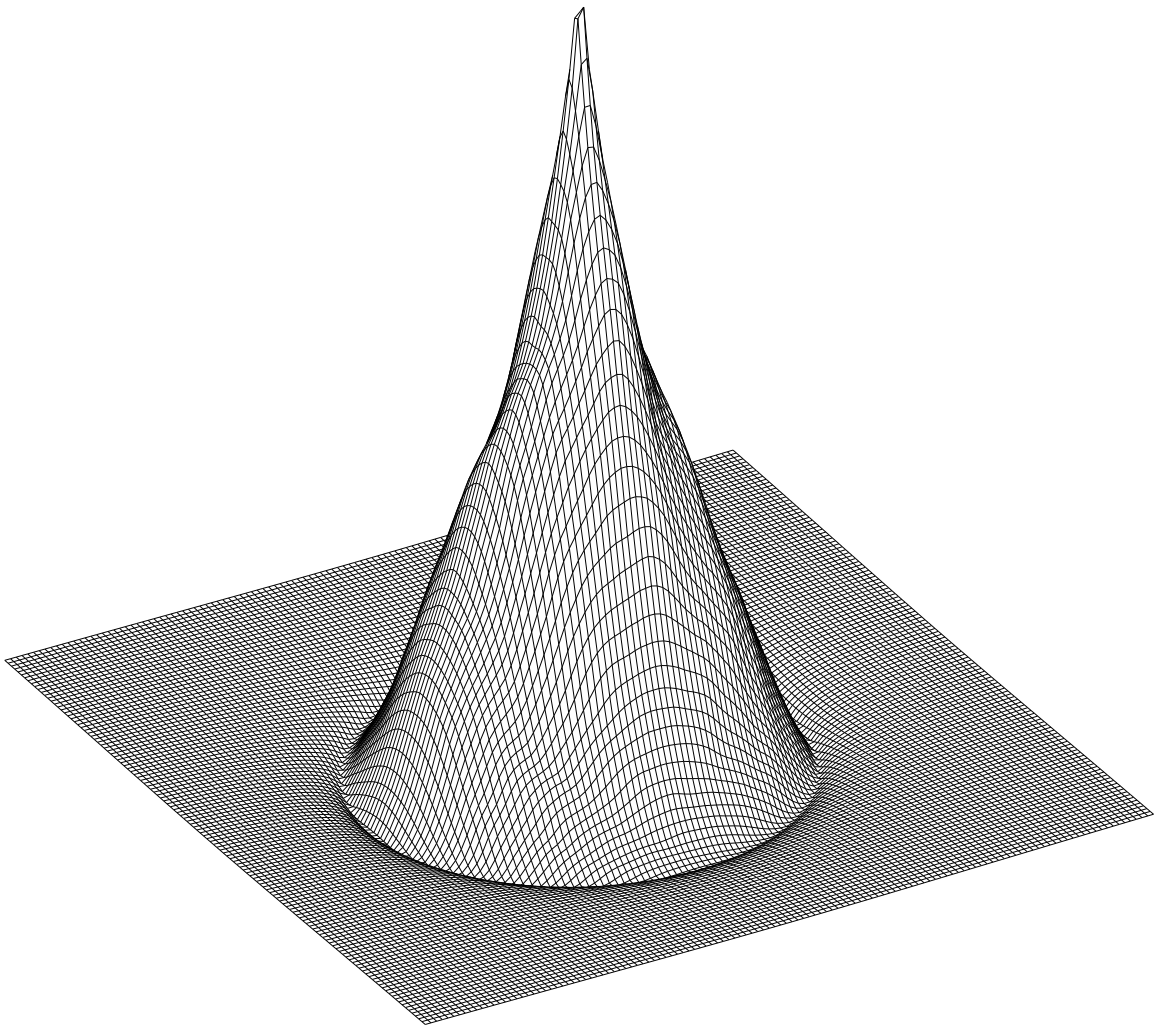

Figure 2: Shadow band spatial correlation function for the full moon.

A sensible model for the spatio-temporal correlation function is a sum over layers:

$$\xi(\mathbf{x},t) = \frac{\alpha\Omega^{-1/3}\sec^{2/3}\zeta}{4\pi^2}\sum_l A_l\xi_p((\mathbf{x}-\mathbf{v}_l t)/\Omega h_l \sec\zeta)F(t/\tau_l) \tag{19}$$

where $A_l = \Delta h C_n^2(h)h^{-1/3}$ and $F(t/\tau_l)$ describes the decorrelation arising from eddy turnover. The correct form of this function can be determined empirically. This equation is valid in the limit of a point like detector, or equivalently, for seeing generated at heights greater than a few metres.

2.6 Confusion With Other Sources of Extinction

One worry is the possibility of correlated intensity fluctuations arising from extinction from dust, mist or clouds. However, to the extent that we can treat such effects as "passive additives" then we would expect these to have a very different power spectrum: $P \propto k^{-11/3}$ as compared to $P \propto k^{1/3}$ for the effect considered here. Extinction would therefore be expected to show large long-range and long-time correlations.

3 Inversion of 1D Correlation Function

The SHABAR correlation function is a sum of patterns like those shown in figure 1 but with different scales according to their distance from the scintillometer. We would like to invert this to get $C_n^2(h)$. One approach is to perform some kind of chi-squared minimization of the deviation of the observed correlation function from the model, possibly with some kind of regularization to enforce smoothness (refs...). Here we explore a different approach.

3.1 Fourier Inversion

In the limit that the detector size can be neglected, the equal time correlation function as obtained from a 1-dimensional SHABAR array can be written as an integral along the line of sight:

$$\xi(x) = \int \frac{dz}{z} A(z)\xi_0(x/z) \tag{20}$$

where $\xi_0(x) = \xi_p(\mathbf{x} = x\mathbf{n}/\Omega \sec\zeta)$ with $\mathbf{n}$ a unit vector along the array, and where

$$A(z) \equiv \alpha\Omega^{-7/3} z^{2/3} C_n^2(z/\sec\zeta)/4\pi^2 \tag{21}$$

The projection (20) can readily be inverted by change of variables from x, z to $\chi = \log x$ and $\rho = \log z$. We then have

$$\xi(\chi) = \int d\rho\, A(\rho)\xi_0(\chi - \rho) \tag{22}$$

where $\xi(\chi) \equiv \xi(x = \exp(\chi))$ and $A(\rho) = A(x = \exp(\rho))$ i.e. the functional form is inferred from whether the argument is greek or latin. This is a simple convolution, so we can obtain the distribution of scintillation strength as a function of log distance $A(\rho)$ by Fourier transforming $\xi(\chi) \to \tilde{\xi}(\kappa) = \int d^2\chi \xi(\chi) e^{i\kappa\chi}$, multiplying by a filter $1/\tilde{\xi}_0(\kappa)$ to obtain

$$\tilde{A}(\kappa) = \tilde{\xi}(\kappa)/\tilde{\xi}_0(\kappa) \tag{23}$$

and then transform back to obtain $A(\rho)$ as a convolution

$$A(\rho) = \int d\chi\, \xi(\chi)\xi_0^{-1}(\chi - \rho) \tag{24}$$

where the convolution kernel $\xi_0^{-1}(\chi)$ is the function whose Fourier transform is the inverse of that of $\xi_0(\chi)$.

3.2 Regularized Fourier Inversion

There is, of course, a problem with this simple prescription: The transform $\tilde{\xi}_0(\kappa)$ becomes very small at high spatial frequency. This may make it difficult to reliably estimate, and, even if this can be done, multiplying by its inverse will strongly amplify high frequency noise in the estimated $\xi(\chi)$. This problem can be overcome by 'softening' the filter and replacing

$$\frac{1}{\tilde{\xi}_0(\kappa)} \to \frac{\tilde{\xi}_0^\star(\kappa)}{|\tilde{\xi}_0(\kappa)|^2 + \epsilon^2} \tag{25}$$

The regularization parameter ϵ stops the inverse filter from blowing up at high frequencies and allows one to control the distance resolving power of the inversion algorithm. The result is a well defined kernel

$$\xi_0^{-1}(\chi) = \int \frac{d\kappa}{2\pi} \frac{\tilde{\xi}_0^\star(\kappa)}{|\tilde{\xi}_0(\kappa)|^2 + \epsilon^2} e^{-i\kappa\chi}. \tag{26}$$

that, when convolved with an estimated correlation function, will give a smoothed version of the true log-distance distribution function $A(\rho)$ with log-distance resolution $\sim 1/\kappa_\star$ where $\kappa_\star$ is such that $|\tilde{\xi}_0(\kappa_\star)| \simeq \epsilon$.

An algorithm for inverting the projection (20) is as follows:

1. Obtain a CCD image of the source $W_{\rm src}(\mathbf{x})$ such as those shown in the left hand panels of figure 1.

2. Compute it's power-spectrum $|\tilde{W}(\mathbf{k})|^2$ and multiply by $k^{1/3}$ and inverse transform to obtain $\xi_p(\mathbf{x})$ (as sshown in the right hand panels of figure 1).

3. Extract a linear sample $\xi_0(x) = \xi_p(x\mathbf{n}/\Omega \sec\zeta)$.

4. Resample this to a logarithmic spacing extending from $x \ll 1$ to $x \gg 1$ and well beyond the range of baselines sampled by the array.

5. Adjust the low x end so that it varies smoothly and has $\xi_0(x_{\rm min}) = \xi_0(x_{\rm max})$ so that we can apply the FFT. In the example shown figure 3 this was done by first adding a constant to set $\xi_0(x_{\rm max}) = 0$ and then multiplying the low x end by half of a cosine wave so that $\xi_0(x)$ tends smoothly to zero as $x \to x_{\rm min}$. This example was for a vertical slice through the correlation function for the full moon (bottom right panel of figure 1).

6. Transform the result, compute $\tilde{\xi}_0^\star(\kappa)/(|\tilde{\xi}_0(\kappa)|^2 + \epsilon)$, and inverse transform to obtain $\xi_0^{-1}(\chi)$.

7. Now take the observed estimates $\hat{\xi}(x)$ obtained from the array. Resample these to equal logarithmic spacing as above, with adjustment of the low x values so that the function wraps smoothly and continuously.

8. Convolve with $\xi_0^{-1}(\chi)$ to obtain $A(\rho)$ and hence $A(z) = A(\rho = \log(z))$.

9. Finally compute $C_n^2(h)$ from (21). Examples of the reconstruction are shown in figure 4.

3.3 Relation To Wiener Filtering

The regularization procedure proposed here is similar to Wiener filtering. The Wiener filter is that which results in an estimate of $\hat{A}(\rho)$ which is as close as possible in a least squares sense to the true profile.

The Wiener filter for this problem is

$$\tilde{A}(\kappa) = \frac{\tilde{\xi}_S^2(\kappa)}{\tilde{\xi}_S^2(\kappa) + \xi_N^2(\kappa)} \frac{\tilde{\xi}(\kappa)}{\tilde{\xi}_0(\kappa)}. \tag{27}$$

This required some estimation of how the ensemble average of the measured correlation function is divided into signal and noise: $\langle\tilde{\xi}^2(\kappa)\rangle = \xi_S^2(\kappa) + \xi_N^2(\kappa)$, which may be difficult, but in the situation that the signal-to-noise ratio becomes small at high spatial frequencies, the Wiener filter has the same general effect as the regularization proposed above that high frequencies are suppressed as compared to the formal inverse. The Wiener filter is a compromize between over-sampling (which results in excessive noise variance) and under-sampling (which results in variance because real high frequency features are suppressed.

Since $\tilde{\xi}_S^2(\kappa) = \tilde{A}^2(\kappa)\tilde{\xi}_0^2(\kappa)$, the Wiener filter is equivalent to the regularized filter if $\tilde{\xi}_N^2(\kappa) = \epsilon^2\tilde{A}^2(\kappa)$. These approaches are equivalent if both the noise and A have white spectra.

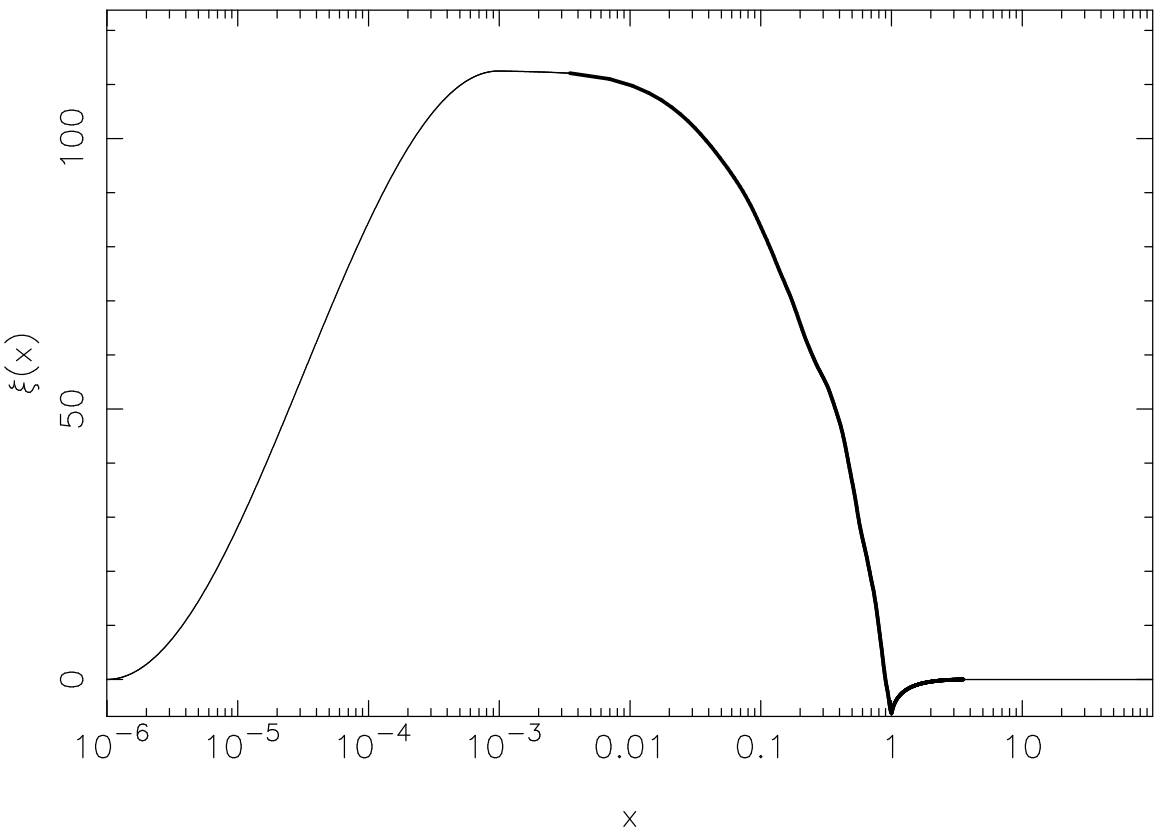

Figure 3: Illustration of re-sampling of a slice through 2-D correlation function computed from a CCD image of the moon into equally space logarithmic interval. The source image is shown in the bottom right panel of figure 1. Computed values are indicated by the thick line. Smoothly interpolated values have been generated to allow use of numerical FFT in log-position coordinates.

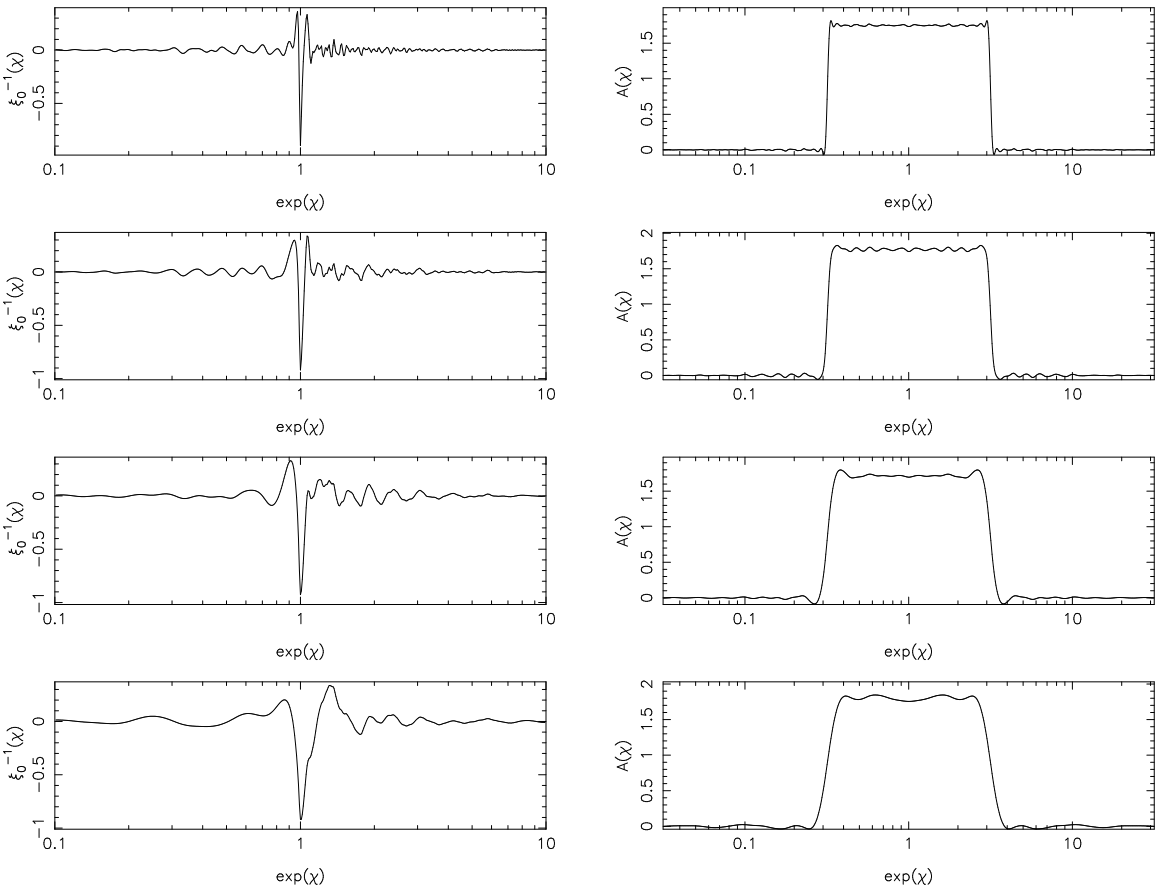

Figure 4: Illustration of regularized Fourier inversion of 1D SHABAR correlation function to obtain $C_n^2(h)$. Left hand panels show the kernel $\xi_0^{-1}(\chi)$ for a variety of values of the regularization parameter. On the right are shown the reconstructed $A(\rho)$ for noise-free data corresponding to a box-car.

3.4 An Approximate Inversion Alorithm

The Fourier inversion technique involves convolving with an extended function, and therefore requires measurements of the SBSCF over a wide range of log-separation. Here we investigate an alternative approximate 1-D inversion algorithm that involves convolution with a kernel with more compact support. This algorithm is stimulated by the observation that, for the full or gibbous moon, the SBSCF is a cone with relatively uniformly sloping sides for $x < D$, but the slope then changes dramatically and, aside from a slight ringing, then becomes very small (see figure 2). The ringing is a consequence of the positive spectral index $n = 1/3$ for the wavefront Laplacian power spectrum. Had we assumed a k^{-4} spectrum for the refractive index rather than $k^{-11/3}$ then the Laplacian would have a white spectrum and the SBSCF would be simply the overlap integral, and would be identically zero for $x > D$. Thus, this sharp feature is primarily a consequence of the shape of the object, and not much affected by the precise form of the refractive index fluctuations. If we take a radial slice through the SBSCF for a single layer at distance z then the second derivative $\xi''(x)$ will be particularly strong for $x = \Omega z$. This suggests that some kind of smoothed second derivative of the SBSCF might provide a useful approximate quasi-local estimator of the scintillation strength profile.

The contribution to $\xi''(x)$ from an interval of heights dh is

$$d\xi''(x) = \frac{\alpha}{4\pi^2} \sec^{2/3}\zeta \Omega^{-7/3} C_n^2(h) h^{-1/3} dh \frac{d^2\xi_0(x/h\Omega\sec\zeta)}{dx^2} \tag{28}$$

Now if we model $\xi_0''(y) = d^2\xi_0(y)/dy^2$ as $\xi_0''(y) = a\delta(y-1)$ with a some constant (i.e. the second derivative is strongly localised around $y = 1$) we have

$$\xi''(x) = \frac{a\alpha}{4\pi^2}\Omega^{-16/3}\sec^{-7/3}\zeta x \int \frac{dy}{y^2}\, C_n^2(x/y\Omega\sec\zeta)(x/y\Omega\sec\zeta)^{-7/3}\delta(y-1) \tag{29}$$

and performing the integral yields

$$x^2\xi''(x) = \frac{a\alpha}{4\pi^2}\Omega^{-7/3}\sec^{2/3}\zeta \left[h^{2/3}C_n^2(h)\right]_{h=x/\Omega\sec\zeta}. \tag{30}$$

In this model, applying the dimensionless operator x^2d^2/dx^2 to $\xi(x)$ yeilds an estimate of $h^{2/3}C_n^2(h)$, the contribution to the scintillation strength per log interval of height. This in turn provides us with an estimate of $C_n^2(x)$.

Since we have noisy data, direct differentiation of the estimated $\hat{\xi}(x)$ is not useful, but (30) suggests that x^2 times some kind of smoothed second derivative operator might give a practical estimator. One possibility is to estimate $\xi''(x)$ by convolving with the second derivative of a Gaussian and to define

$$A(x) = \frac{x^2}{\sigma^2(x)} \int \frac{dx'}{\sqrt{2\pi}\sigma(x)} \left(\frac{x'^2}{\sigma^2(x)} - 1\right) e^{-x'^2/2\sigma^2(x)} \hat{\xi}(x - x') \tag{31}$$

with $\sigma(x) = \alpha x$ and with α some moderately small number that sets the resolution. This tends to $x^2\xi''(x)$ as $\alpha \to 0$. This model is only an approximation, of course, since the true $\xi''(x)$ is not a pure delta function. Consequently, the response of $A(x)$ to a single refractive layer will not be a delta function at $x = \Omega h \sec\zeta$, but will generally show some false signal at other x values, so there will be aliasing. The estimator has been constructed so that as we vary the height of the layer the response, plotted in logarithmic coordinate, maintains it's shape. In figure 5 we show how well this works in practice. In the left hand panels we show the response to a single layer at height $h = 1$ for various smoothing parameters.

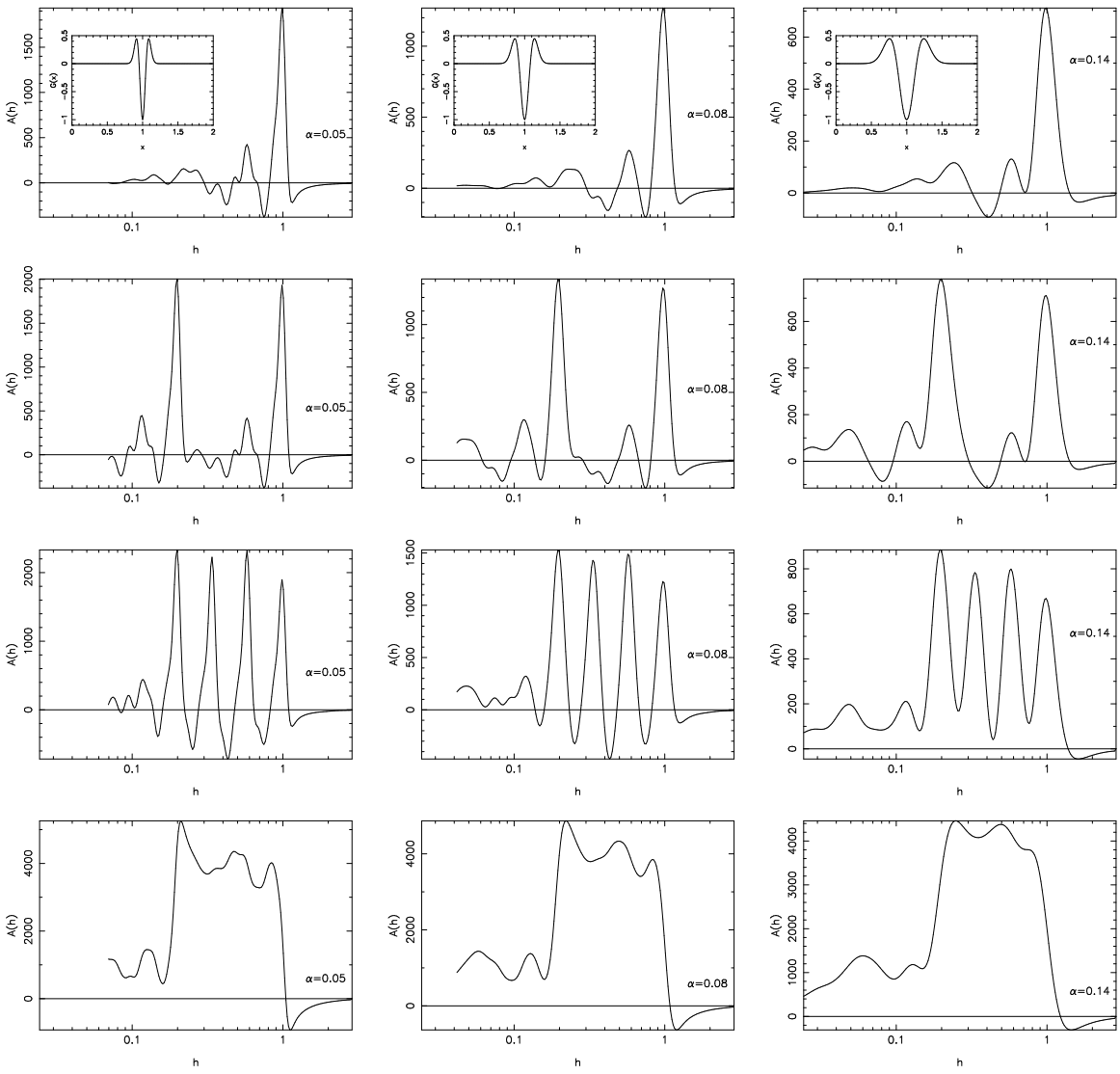

Figure 5: Left hand panels show the response of the scintillation strength estimator defined in (31) to a single refractive layer. There is a nice strong spike, but there also side-lobes. The inset plots show, on a linear scale, the smoothing kernels. The central and right hand panels show 3 and 10 layers respectively. The layers are equally spaced in log height and have equal (lunar) scintillation strength. It would appear that the estimator should give an estimate of the scintillation, and hence C_n^2, profile good to perhaps 15%.

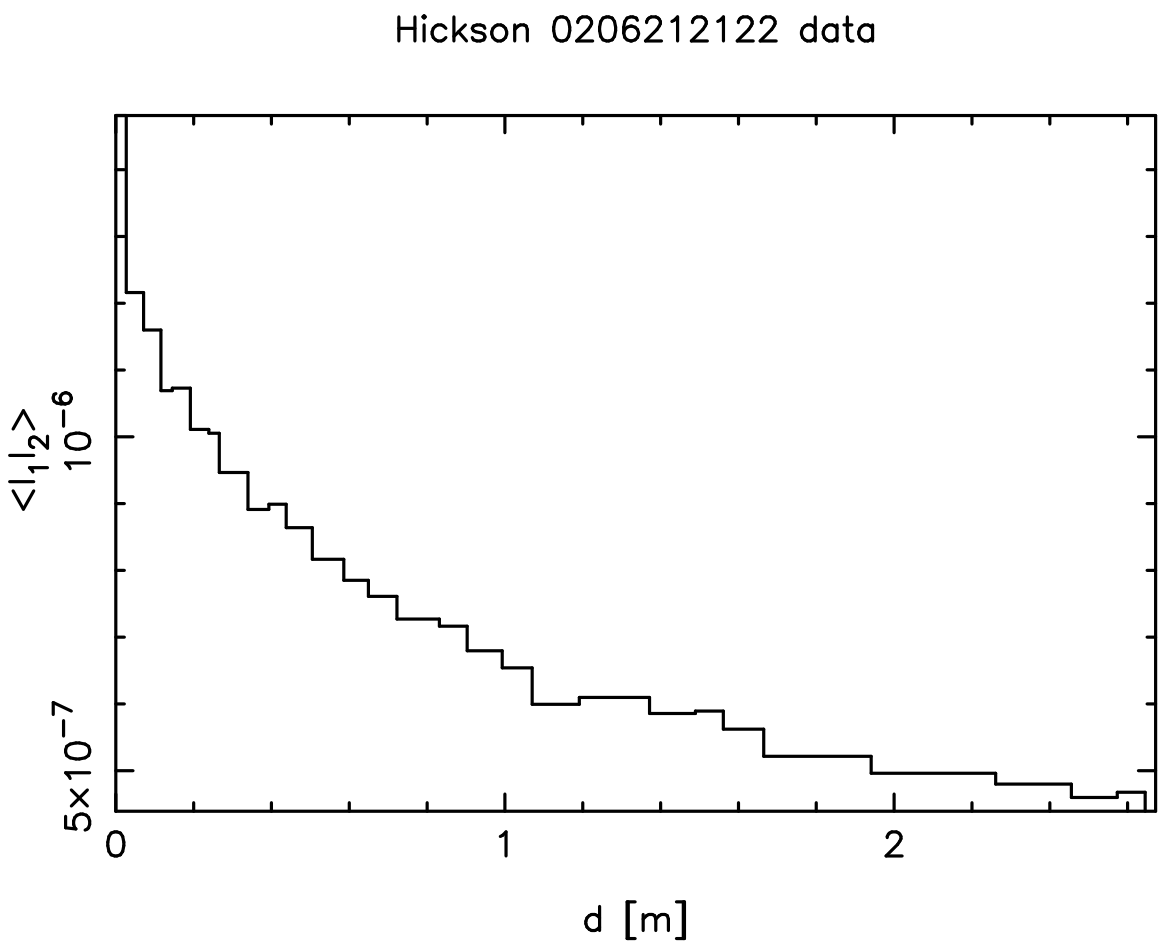

Figure 6: Shadow band auto-correlation function measured by Paul Hickson.

4 Hickson's Results

Paul Hickson at UBC has constructed and successfully deployed a lunar SHABAR scintillometer array. He used 1cm diameter avalanche photo-diodes (APDs) with a range of baselines from 5.4cm to 2.67m. Illuminated by the full moon, these generate $\sim 2 \times 10^{11}$ photo-electrons per second. Example results are shown in figure 6. The bandwidth of his system is 500Hz, and he plans to increase this to 1kHz.

Hickson has also developed an inversion algorithm.

5 Signal To Noise

Let the average lunar illumination generate photo-electrons at a rate R. The rms shot-noise fluctuation in the intensity averaged over a sample time Δt is $\Delta I_{\rm SN} = (R\Delta t)^{-1/2}$. If we take a series of N pairs of samples from two independent detectors with separation $\mathbf{d}$, we can multiply them and average to obtain an estimator of the correlation function:

$$\hat{\xi}(\mathbf{d}) = \frac{1}{N}\sum \Delta I_1 \Delta I_2. \tag{32}$$

In the absence of any signal, this is the sum of N independent random variates $\Delta I_1 \Delta I_2$ with zero mean and typical value $\Delta I^2_{\rm SN} = 1/(R\Delta t)$, resulting in rms fluctuations in the estimator

$$\sigma_\xi \equiv \langle \Delta\xi(\mathbf{d})^2\rangle^{1/2} \sim \frac{1}{\sqrt{N}R\Delta t} = (R\sqrt{\tau\Delta t})^{-1} \tag{33}$$

where $\tau = N\Delta t$ is the averaging time. The fluctuation in the correlation function on the order of the inverse square root of the number of photo-electrons generated in a time $\sqrt{\tau\Delta t}$. This becomes large if we make the sampling time very short. However, for fluctuations arising from height h, the time-scale for intensity fluctuations is $\tau(h,v) \sim \Omega h/v \sim 10{\rm ms}\ h_{10}/v_{10}$ with $h_{10} = h/10{\rm m}$ and $v_{10} = v/10{\rm m/s}$, and we can afford to take the sampling time to be $\lesssim \tau(h,v)$ (or rebin) and the limiting statistical uncertainty is $\sigma_\xi(h) \sim 1/R\sqrt{\tau\Omega h/v}$.

For a mm size detector we expect $R \simeq 10^9$/s, so, for a sample time of 1ms and averaging over 10 seconds we obtain a statistical uncertainty $\sigma_\xi \sim 10^{-8}$, as compared to an expected signal $\xi \sim 10^{-6}$. The uncertainty in the intensity, averaged over an interval $\sim \tau(h,v)$ is $\sigma_I \sim \sqrt{R\tau(h,v)} \sim 3\times 10^{-5}$. This is quite comparable to the actual signal. This means that if one were to use a larger detector then the statistical uncertainty would be smaller, but the true uncertainty in the ensemble average correlation function would then be limited by the finite number of independent realizations rather than by photon counting statistics. A 1mm size detector is therefore well matched to the expected signal amplitude. Since a small detector is advantageous, especially if using the crescent moon, this size is probably close to optimal.

It would be desirable to develop a method for fitting a model of the form 19 to estimates of the spatio-temporal correlation function $\hat{\xi}(\mathbf{x},t)$. This has non-trivial impact on the choice of spacing of the scintillometers.

References

Beckers, J. M. 1993, Sol. Phys., 145, 399

—. 2001, Experimental Astronomy, 12, 1

Roddier, F. 1981, Progress in Optics. Volume 19. Amsterdam, North-Holland Publishing Co., 19, 281

Seykora, E. J. 1993, Sol. Phys., 145, 389